J. Fluid Mech. (1987), *vol.* 178, *pp.* 257–277
Printed in Great Britain

A two-equation model for contaminant dispersion in natural streams

By RONALD SMITH

Department of Applied Mathematics and Theoretical Physics,
University of Cambridge, Silver Street, Cambridge CB3 9EW, UK

(Received 9 June 1986)

A simple two-equation model is derived which has the properties that the total contaminant exposure, the mean time of arrival, the temporal spread, and the skewness, are asymptotically correct at large distances downstream of a discharge. The role of changes in the breadth of a river upon the dispersion process is investigated by a means of an illustrative example. This reveals cubic dependence upon the breadth, and hence the great importance of wide reaches of rivers as regards contaminant dispersion.

1. Introduction

There have been two principal lines of development in the mathematical modelling of contaminant dispersion in streams: hydrodynamics, and time-series analysis. The concerns of hydrodynamics are to understand and to quantify the processes whereby dilution in rivers is so remarkably efficient. An intrinsic limitation is that the variability of the geometry in natural streams precludes the accurate application of any model based upon the detailed fluid mechanics. Moreover, it is only recently that analytical models of sufficient complexity have begun to be developed (Smith 1983). Time-series analysis uses observed concentrations in the river to construct robust predictive schemes. The limitations are those of the data. Thus, for other discharges or flow conditions, the predictions might be unreliable. For example, in China the flow of the Yangtze will be reduced during the prolonged construction of a hydroelectric scheme. The vulnerability to pollution will be most when the ability to predict it is least.

Fortunately, this seems to be an era of convergence between the two mathematical traditions. For example, Chatwin (1980) shows how his earlier hydrodynamic study (Chatwin 1970) can be adapted to analyse field data. From the other side of the divide, Beer & Young (1983) apply time-series parameter estimation to a dead-zone model of the dilution process:

$$\partial_t c + u\,\partial_x c = \alpha(s-c), \tag{1.1a}$$

$$\partial_t s = \beta(c-s). \tag{1.1b}$$

The first equation describes the main flow with concentration c and velocity u, and the second equation describes the stagnant pockets with concentration s. The exchange parameters α, β relate to the relative volume of the stagnant pockets and to the mixing process. Variability along the river is accounted for by permitting the three adjustable parameters u, α, β to vary from reach to reach of the river. The concentration profiles predicted by Chatwin (1980) or by Beer & Young (1983) share

the feature of marked skewness, which has long been recognized as a distinctive feature for contaminant dispersion in rivers (Nordin & Sabol 1974).

In this spirit of reconciliation, the purpose of the present paper is to derive a model of the form (1.1*a*, *b*) from the detailed hydrodynamics. For uniform flows, Smith (1981, §5) has derived such a model, with the minor change that both zones have non-zero velocities. Here we encompass the non-uniformity of natural streams.

Once the model equations have been derived, secondary questions are how do the coefficients vary with changing river flow rate, and which reaches of the river are most important as regards contaminant dispersion? These questions are answered by means of simple illustrative examples. The counterparts to the above coefficients u, α, β are found to be approximately proportional to the river volume flow rate. The relative importance upon the dispersion process of different reaches of the river varies as the cube of the width. Hence, field observations or any other modelling effort, should be weighted towards the wider, slower-flowing reaches of a river.

2. Advection–diffusion equation

In a river, advection velocities are typically a factor of 15 larger than turbulent velocities. One consequence is that along the flow (systematic) advection vastly dominates (random-walk) turbulent diffusion. Thus, in axes aligned along and across the flow (see figure 1), longitudinal diffusion can be neglected. A second consequence is that vertical mixing has an e-folding distance of the order of 15 water depths downstream. On the assumptions that this is much shorter than the horizontal lengthscale for changes in the river profile, and that the river is much wider than it is deep, we shall regard the contaminant as being vertically well mixed.

In view of the above considerations, we commence our analysis of contaminant dispersion in natural streams with the vertically averaged two-dimensional advection–diffusion equation:

$$m_1 m_2 h(\partial_t c + u\,\partial_x c) - \partial_y\left(\frac{m_1}{m_2} h\kappa\,\partial_y c\right) = m_1 m_2 hq, \tag{2.1a}$$

with

$$h\kappa\,\partial_y c = 0 \quad \text{on } y = y_{\mathrm{L}}, y_{\mathrm{R}}, \tag{2.1b}$$

and

$$\partial_x (m_1 m_2 hu) = 0. \tag{2.2}$$

Here (x, y) are curvilinear coordinates aligned along and across the flow (Yotsukura & Sayre 1976), m_1, m_2 are metric coefficients (see figure 1), $c(x, y, t)$ is the contaminant concentration, h the water depth, u the rate of crossing of x-contours (the velocity is $m_1 u$), κ the transverse diffusion coefficient, q the depth-averaged source strength, and $y_{\mathrm{L}}, y_{\mathrm{R}}$ the left and right banks of the stream. Secondary circulation, such as that due to bends, has been averaged out, i.e. the contribution to the cross-stream diffusion process is allowed for by an appropriate modification to κ (Fischer 1969).

The above equations have been studied at great length by the author (Smith 1983, 1984). Two useful averages are the cross-section average

$$\bar{f} = \int_{y_{\mathrm{R}}}^{y_{\mathrm{L}}} m_1 m_2 hf\,\mathrm{d}y \Big/ \int_{y_{\mathrm{R}}}^{y_{\mathrm{L}}} m_1 m_2 h\,\mathrm{d}y, \tag{2.3}$$

and the flow-weighted average

$$[f] = \int_{y_{\mathrm{R}}}^{y_{\mathrm{L}}} m_1 m_2 huf\,\mathrm{d}y \Big/ \int_{y_{\mathrm{R}}}^{y_{\mathrm{L}}} m_1 m_2 hu\,\mathrm{d}y. \tag{2.4}$$

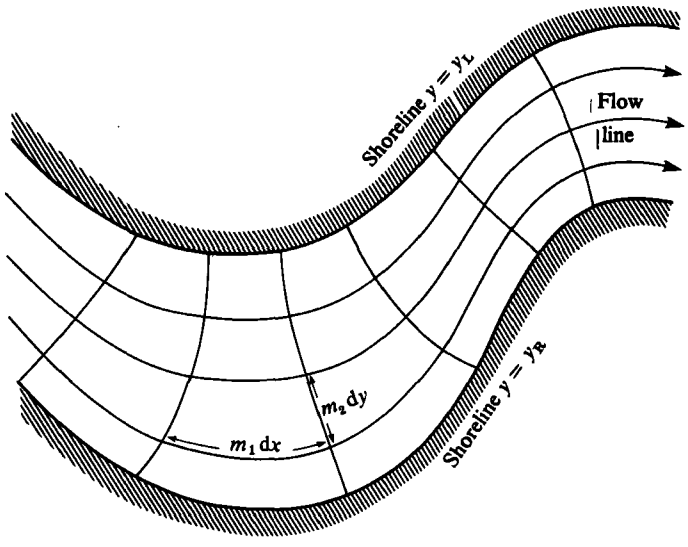

FIGURE 1. Flow-following coordinate system for a meandering channel.

With a slight abuse of notation, we write

$$\overline{m}_1 = \frac{1}{A}\int_{y_R}^{y_L} m_1 m_2 h\,dy, \tag{2.5a}$$

where

$$A = \int_{y_R}^{y_L} m_2 h\,dy \tag{2.5b}$$

is the cross-sectional area. The integrated form of the mass-conservation equation (2.2) can then be written

$$\overline{m}_1 \overline{u}_1 A = F = \text{constant}, \tag{2.6}$$

where F is the river volume flow rate. The conventional choice of x-coordinate is to make $\overline{m}_1 = 1$. However, in §8 we find the extra freedom of a distorted longitudinal coordinate can be useful.

3. Moments and the time-lag functions

The major virtue of the two-zone model proposed by Smith (1981, §5) is that it reproduces many asymptotic (large-time) properties of the spatial moments. For longitudinally varying flows such moments with respect to x cannot be used. However, Smith (1984) gives corresponding asymptotic (large-distance) results for temporal moments:

$$c^{(j)}(x,y) = \int_{-\infty}^{\infty} \tau^j c(x,y,t)\,dt, \tag{3.1}$$

where τ is a displaced time coordinate relative to the mean travel time from the source position $x = x_0$:

$$\tau = t - \int_{x_0}^{x} \frac{dx'}{\overline{u}(x')}. \tag{3.2}$$

For a discharge at $t=0, x=x_0$ with cross-stream profile $q(y_0)$, Smith (1984, equation (4.9)) shows that at a far-downstream location (x,y), the centroid time of arrival is

$$T=\left(\frac{\overline{qG_-}}{\bar{q}}\right)_{x_0}+G_+(x,y). \tag{3.3}$$

Here the downstream and upstream time-lag functions G_+, G_- satisfy the advection–diffusion equations

$$m_1 m_2 hu\,\partial_x G_+ - \partial_y\left(\frac{m_1}{m_2}hk\,\partial_y G_+\right)=m_1 m_2 h\left(1-\frac{u}{\bar{u}}\right), \tag{3.4a}$$

$$-m_1 m_2 hu\,\partial_x G_- - \partial_y\left(\frac{m_1}{m_2}hk\,\partial_y G_-\right)=m_1 m_2 h\left(1-\frac{u}{\bar{u}}\right), \tag{3.4b}$$

with

$$hk\,\partial_y G_+ = hk\,\partial_y G_- = 0 \quad \text{on } y=y_L, y_R \tag{3.4c}$$

and

$$[G_+]=[G_-]=0. \tag{3.4d}$$

The absence of time derivatives makes these equations for G_+, G_- an order-of-magnitude easier to solve than (2.1a, b) for $c(x,y,t)$. For example, the NAG computer routine D03 BPF is directly applicable to (3.4). Thus, we shall regard G_+ and G_- as being known. Qualitatively, the cross-stream structure of G_+ and G_- can be inferred from the forcing term $(1-u/\bar{u})$. In the slow-moving water at the sides of the river, the forcing term is positive and there is a time lag (G_+ and G_- are positive). While, in the fast-moving water at the centre, the forcing term is negative and there is early arrival (G_+ and G_- are negative).

For the particular case of a discharge proportional to the local river flow $u/\bar{u}$, the temporal variance Σ_T^2 of $[c]$ at large distances downstream can likewise be related to these same functions G_+, G_-:

$$\Sigma_T^2 = 2\int_{x_0}^{x}\frac{\bar{G}_+}{\bar{u}}\,\mathrm{d}x' - 2[G_+ G_-]_{x_0} \tag{3.5}$$

(Smith 1984, equation (6.10)). The integral term allows us to evaluate the effective longitudinal diffusivity (shear-dispersion coefficient):

$$D=\overline{m_1^2}\,\bar{u}^2\,\bar{G}_+. \tag{3.6}$$

The inclusion of the $\overline{m_1^2}$ factor in the definition (3.6) makes D independent of the choice of x-coordinate. The x_0 term in (3.5) relates to the initial inefficiency of the longitudinal dispersion process in the convective region.

The familiar role of D is in a diffusion model for the shear-dispersion process

$$A(\partial_t \bar{c}+\bar{u}\,\partial_x \bar{c})-\frac{1}{\overline{m_1}}\partial_x\left(\frac{AD}{\overline{m_1}}\partial_x \bar{c}\right)=\bar{q} \tag{3.7}$$

(Taylor 1953).

For the third moment (relative to the displaced time of arrival T), a key role is again played by the functions G_+, G_- (Smith 1984, §10):

$$\frac{1}{[c^{(0)}]}\int_{-\infty}^{\infty}(\tau-T)^3[c]\,\mathrm{d}t \approx 6\int_{x_0}^{x}(\overline{G_+G_-}-[G_+G_-])\frac{\mathrm{d}x'}{\bar{u}}+\text{constant}. \tag{3.8}$$

The constant term depends upon the discharge position x_0 and the profile q. Usually $\overline{G_+G_-} > [G_+G_-]$, so the third moment increases with $x-x_0$. The corresponding linear

growth (3.5) of the second moment implies that the skewness with respect to time is positive with slow decay as $(x-x_0)^{-\frac{1}{2}}$ (Chatwin 1980). It is the marked skewness of the observed contaminant distributions (Nordin & Sabol 1974) that invalidates the use of classical diffusion models of the dispersion process (Taylor 1953).

The above results ((3.3), (3.5), (3.8)) establish that the two functions G_+, G_- provide the ingredients for a good asymptotic model for the dispersion process. To see how to use those ingredients, the next section explores the exact structure of the solution for the concentration $c(x, y, t)$. Readers more concerned with the results than with derivations can turn to §6, where the eventual two-equation model is stated.

4. Spatial eigenmodes

A useful interpretation of the two-zone model proposed by Smith (1981, §5), is a two-mode truncation of the full advection–diffusion equation. For non-uniform flows there are not temporal modes as used by Smith (1981). However, there are spatial modes (Smith 1983, §7) which satisfy the equations

$$\partial_y\left(\frac{m_1}{m_2}hk\,\partial_y\phi_n^{(+)}\right)+\overline{m}_1\mu_n m_1 m_2 hu\phi_n^{(+)}=m_1 m_2 hu\,\partial_x\phi_n^{(+)}, \tag{4.1a}$$

$$\partial_y\left(\frac{m_1}{m_2}hk\,\partial_y\phi_n^{(-)}\right)+\overline{m}_1\mu_n m_1 m_2 hu\phi_n^{(-)}=-m_1 m_2 hu\,\partial_x\phi_n^{(-)}, \tag{4.1b}$$

with

$$hk\,\partial_y\phi_n^{(+)}=hk\,\partial_y\phi_n^{(-)}=0 \quad \text{on } y=y_{\mathrm{L}}, y_{\mathrm{R}}, \tag{4.1c}$$

$$[\phi_n^{(+)}\phi_n^{(-)}]=1, \tag{4.1d}$$

$$[\phi_n^{(+)}\phi_j^{(-)}]=0 \quad (n\neq j), \tag{4.1e}$$

$$[\phi_n^{(+)}\partial_x\phi_n^{(-)}]=[\phi_n^{(-)}\partial_x\phi_n^{(+)}]=0. \tag{4.1f}$$

The $\overline{m}_1$ factors in (4.1*a*, *b*) have been included to make μ_n independent of the choice of x-coordinate. The lowest mode is

$$\phi_0^{(+)}=\phi_0^{(-)}=1, \quad \text{with } \mu_0=0, \tag{4.2}$$

corresponding to uniform concentration across the flow. The constraint (4.1*f*) minimizes the x-dependence of the modes, so that in the limiting case of uniform flows the adjoint upstream and downstream modes $\phi_n^{(-)}, \phi_n^{(+)}$ become identical.

To incorporate the time dependence of the concentration and discharge strength, we define

$$c=\sum_{n=0}^{\infty} c_n(x,t)\,\phi_n^{(+)}(x,y), \quad c_n=[c\phi_n^{(-)}], \tag{4.3a, b}$$

$$q=\frac{u}{\overline{u}}\sum_{n=0}^{\infty} q_n(x,t)\,\phi_n^{(+)}(x,y), \quad q_n=\overline{q\phi_n^{(-)}}. \tag{4.4a, b}$$

Thus, the $\phi_n^{(+)}$ component of (2.1*a*, *b*) becomes

$$\overline{u}(\partial_x c_n+\overline{m}_1\mu_n c_n)=q_n-\sum_{j=0}^{\infty}\overline{\phi_j^{(+)}\phi_n^{(-)}}\,\partial_t c_j. \tag{4.5}$$

We can infer from (4.5) that downstream of the source, the convergence of the series (4.3*a*) for c becomes quite rapid. First, the eigenvalues μ_n grow as n^2. Secondly, the increasingly oscillatory structure of the higher modes $\phi_n^{(+)}, \phi_n^{(-)}$ implies that the

off-diagonal coefficients $\overline{\phi_j^{(+)}\phi_n^{(-)}}$ decay as n^{-1}. Hence, the overall rate of decay of the c_n coefficients is as n^{-3}. A detailed evaluation of the coefficients, which conforms to these general trends, is given in (8.2*a*, *b*).

The rapid convergence suggests that reasonable results might be obtained with a truncated set of equations. Indeed, a direct two-mode truncation $n = 0, 1$ of (4.5) yields a pair of equations similar to the dead-zone model (1.1). To improve upon the accuracy of this truncation in the longitudinally uniform case, Smith (1981, §5) replaces the ϕ_1 mode and the decay rate μ_1 by choices which lead to optimal accuracy at large times. The objective of the present paper is to do likewise for non-uniform flows.

5. Choosing the approximate modes

The results quoted in §3 show that if an approximation correctly reproduces the time-lag functions G_+, G_-, then it will automatically yield accurate asymptotic results for the temporal centroid, variance and skewness. Thus, exact representations for G_+, G_- provide a starting point for the derivation of approximations:

$$G_+ = \sum_{n=1}^{\infty} t_n^{(+)}(x)\,\phi_n^{(+)}(x,y), \quad G_- = \sum_{n=1}^{\infty} t_n^{(-)}(x)\,\phi_n^{(-)}(x,y), \tag{5.1a, b}$$

with

$$t_n^{(+)} = \int_{-\infty}^{x} \frac{\overline{\phi_n^{(-)}}(x')}{\overline{u}(x')} \exp\Big(-\int_{x'}^{x} \mu_n(x'')\,\overline{m}_1\,\mathrm{d}x''\Big)\,\mathrm{d}x', \tag{5.1c}$$

$$t_n^{(-)} = \int_{x}^{\infty} \frac{\overline{\phi_n^{(+)}}(x')}{\overline{u}(x')} \exp\Big(-\int_{x}^{x'} \mu_n(x'')\,\overline{m}_1\,\mathrm{d}x''\Big)\,\mathrm{d}x' \tag{5.1d}$$

(Smith 1983, equation (7.6)). The use of the t_n notation alludes to the time dimensionality of the coefficients.

For later use, we note the formulae

$$[G_+\,G_-] = \sum_{n=1}^{\infty} t_n^{(+)}\,t_n^{(-)}, \tag{5.2a}$$

$$\overline{G_+} = \sum_{n=1}^{\infty} t_n^{(+)}\,\overline{\phi_n^{(+)}}, \quad \overline{G_-} = \sum_{n=1}^{\infty} t_n^{(-)}\,\overline{\phi_n^{(-)}}, \tag{5.2b, c}$$

$$\overline{\kappa\,\partial_y G_+\,\partial_y G_-} = \overline{u}\,\overline{m}_1 \sum_{n=1}^{\infty} \mu_n\,t_n^{(+)}\,t_n^{(-)}, \tag{5.2d}$$

$$[G_+\,\partial_x G_-] - [G_-\,\partial_x G_+] = \sum_{n=1}^{\infty} (t_n^{(+)}\,\partial_x t_n^{(-)} - t_n^{(-)}\,\partial_x t_n^{(+)}), \tag{5.2e}$$

$$\overline{G_+\,G_-} = \sum_{m=1}^{\infty}\sum_{n=1}^{\infty} t_m^{(+)}\,t_n^{(-)}\,\overline{\phi_m^{(+)}\,\phi_n^{(-)}}. \tag{5.2f}$$

As remarked in §3, it is comparatively easy to compute G_+, G_-. Thus, we shall regard these functions as being known, and we pose the one-mode approximation

$$\boldsymbol{\Phi}_+(x,y) = \frac{G_+(x,y)}{T_+(x)}, \quad \boldsymbol{\Phi}_-(x,y) = \frac{G_-(x,y)}{T_-(x)}, \tag{5.3a, b}$$

with

$$\partial_x T_+ + \overline{m}_1\,\mu T_+ = \frac{\overline{\boldsymbol{\Phi}}_-}{\overline{u}}, \quad -\partial_x T_- + \overline{m}_1\,\mu T_- = \frac{\overline{\boldsymbol{\Phi}}_+}{\overline{u}}, \tag{5.3c, d}$$

and $$[\Phi_+ \Phi_-] = 1, \quad \text{i.e. } T_+ T_- = [G_+ G_-]. \tag{5.3e}$$

The corresponding truncated version of (4.5) is

$$\partial_t[c] + \overline{u}\,\partial_x[c] = \overline{q} - \overline{\Phi}_+ \partial_t c_1, \tag{5.4a}$$

$$\frac{\overline{G_+ G_-}}{[G_+ G_-]} \partial_t c_1 + \overline{u}(\partial_x c_1 + \overline{m}_1 \mu c_1) = \overline{q\Phi_-} - \overline{\Phi}_- \partial_t[c]. \tag{5.4b}$$

If we multiply (3.4*a*, *b*) respectively by G_-, G_+ and average across the flow, we can derive the identities

$$\overline{\kappa\,\partial_y G_+ \partial_y G_-} = \overline{G}_- - \overline{u}[G_- \partial_x G_+] = \overline{G}_+ + \overline{u}[G_+ \partial_x G_-]. \tag{5.5}$$

These enable us to confirm the compatibility between the product formula (5.3*e*) and the ordinary differential equations (5.3*c*, *d*).

To fully determine the coefficients $\overline{\Phi}_+, \overline{\Phi}_-, \mu$, we need a further constraint. Instead of seeking yet another exact property of the concentration distribution, we choose instead to simplify the model equations (5.4*a*, *b*). Specifically, we equate the two coupling coefficients, i.e. $\overline{\Phi}_+ = \overline{\Phi}_-$. This leads to the formulae

$$\overline{\Phi}_+ = \overline{\Phi}_- = \left(\frac{\overline{G}_+ \overline{G}_-}{[G_+ G_-]}\right)^{\frac{1}{2}}, \tag{5.6a}$$

$$T_+ = [G_+ G_-]^{\frac{1}{2}} \left(\frac{\overline{G}_+}{\overline{G}_-}\right)^{\frac{1}{2}}, \quad T_- = [G_+ G_-]^{\frac{1}{2}} \left(\frac{\overline{G}_-}{\overline{G}_+}\right)^{\frac{1}{2}}, \tag{5.6b, c}$$

$$\mu = \frac{\overline{\kappa\,\partial_y G_+ \partial_y G_-} - \frac{1}{2}\overline{u}[G_+ \partial_x G_- - G_- \partial_x G_+]}{\overline{m}_1\,\overline{u}[G_+ G_+]} + \frac{1}{2\overline{m}_1}\left(\frac{\partial_x \overline{G}_-}{\overline{G}_-} - \frac{\partial_x \overline{G}_+}{\overline{G}_+}\right). \tag{5.6d}$$

6. Two-equation model

The outcome of the analysis of the previous two sections is the pair of equations

$$\partial_t[c] + \overline{u}\,\partial_x[c] = \overline{q} - \left(\frac{\overline{G}_+ \overline{G}_-}{[G_+ G_-]}\right)^{\frac{1}{2}} \partial_t c_1, \tag{6.1a}$$

$$\frac{\overline{G_+ G_-}}{[G_+ G_-]} \partial_t c_1 + \overline{u}(\partial_x c_1 + \overline{m}_1 \mu c_1) = q_1 - \left(\frac{\overline{G}_+ \overline{G}_-}{[G_+ G_-]}\right)^{\frac{1}{2}} \partial_t[c], \tag{6.1b}$$

where

$$q_1 = \overline{qG_-}\left(\frac{\overline{G}_+}{\overline{G}_-[G_+ G_-]}\right)^{\frac{1}{2}}. \tag{6.1c}$$

Here c_1 is a measure of the concentration non-uniformity across the river, and q_1 is the corresponding non-uniformity of the discharge. The time-lag functions $G_+(x, y), G_-(x, y)$ are defined in (3.4*a*–*d*) and the spatial decay rate μ is given by the formulae

$$\begin{aligned} \mu &= \frac{\overline{G}_+ + \frac{1}{2}\overline{u}\,\partial_x[G_+ G_-]}{\overline{m}_1\,\overline{u}[G_+ G_-]} + \frac{1}{2\overline{m}_1}\left(\frac{\partial_x \overline{G}_-}{\overline{G}_-} - \frac{\partial_x \overline{G}_+}{\overline{G}_+}\right) \\ &= \frac{\overline{G}_- - \frac{1}{2}\overline{u}\,\partial_x[G_+ G_-]}{\overline{m}_1\,\overline{u}[G_+ G_-]} + \frac{1}{2\overline{m}_1}\left(\frac{\partial_x \overline{G}_-}{\overline{G}_-} - \frac{\partial_x \overline{G}_+}{\overline{G}_+}\right). \end{aligned} \tag{6.2}$$

The implied two-term approximation to the concentration profile across the flow is

$$[c] + c_1 \frac{G_+(x, y)}{[G_+ G_-]^{\frac{1}{2}}} \left(\frac{\overline{G}_-}{\overline{G}_+}\right)^{\frac{1}{2}}. \tag{6.3}$$

Equation (6.1*a*) describes how the uniform contribution [*c*] to the concentration is carried at the bulk velocity $\overline{u}$, and that any spreading is associated with the rate of change of c_1. Equation (6.1*b*) shows that the perturbation from uniformity across the flow is generated via the rate of change of [*c*]. The response takes place over a distance of order $1/\mu$ and tends to be carried along at a velocity

$$u_{11} = \overline{u}\frac{[G_+ G_-]}{\overline{G_+ G_-}}. \tag{6.4}$$

The skewness of the [*c*] contaminant distribution (i.e. the drawn-out tail) can be linked to the slowness of the c_1 mode. Specifically, the $\partial_t c_1$ coefficient in (6.1*b*) is the ratio $\overline{u}/u_{11}$ (i.e. a slowness factor). If this is greater than 1, then (3.8) shows that the temporal skewness is positive, i.e. a rapid surge of concentration when the contaminant arrives at the monitoring position, followed by a more gradual decay.

By construction, for an arbitrary source distribution $q(z, y, t)$, the time-integrated concentration and centroid are exact at large distances downstream. Also, the dominant contributions to the variance and skewness are correct. In the special case in which the discharge strength is proportional to the local river velocity, the variance is exact.

The main advantage of (6.1*a*, *b*) over a more empirical model such as (1.1*a*, *b*) is that the coefficients are properties of the river. Thus, if time-series parameter estimation is used to evaluate the coefficients for one set of discharge conditions, the equations should be equally applicable to other discharge scenarios. Another advantage is that it is possible to infer how the coefficients need to be changed for a different flow rate, or if the depth profile were to be modified by dredging. All that needs to be done is to examine how the functions G_+, G_- are changed.

In the Appendix it is shown that there is an alternative formulation of (6.1*a*, *b*) which corresponds even more closely to the dead-zone model (1.1*a*, *b*).

7. Illustrative example

As a preliminary to the investigation of longitudinal variations of the river breadth, this section concerns the simpler circumstance of longitudinally uniform channels. The river is assumed to comprise a constant-depth central region, and two symmetrical constant-depth side regions, with constant velocities and diffusivities within each region (see figure 2). In practice, the transition of velocity and of diffusivity would take place smoothly over a width comparable with the water depth. Thus, in using an abrupt transition, we are assuming that the river is much wider than it is deep. The depth ratio is denoted $1:r$ and the ratio of volume flow between the central region and the sum of the sides is denoted $1+s:1-s$. Following Smith (1984, appendix B), we relate the velocities and diffusivities respectively to the $\frac{1}{2}$ and $\frac{3}{2}$ powers of the local depth. Hence, the breadths, depths, velocities and diffusivities of the central and side regions have the specifications

$$\left.\begin{array}{ll} B\dfrac{2(1+s)}{1+s+(1-s)r^{-\frac{3}{2}}}, & B\dfrac{(1-s)}{(1+s)r^{\frac{3}{2}}+1-s}, \\ \overline{h}\dfrac{1+s+(1-s)r^{-\frac{3}{2}}}{1+s+(1-s)r^{-\frac{1}{2}}}, & \overline{h}\dfrac{(1+s)r^{\frac{3}{2}}+1-s}{(1+s)r^{\frac{1}{2}}+1-s}, \\ \overline{u}_{\frac{1}{2}}[1+s+(1-s)r^{-\frac{1}{2}}], & \overline{u}_{\frac{1}{2}}[(1+s)r^{\frac{1}{2}}+1-s], \\ K_{\frac{1}{2}}[1+s+(1-s)r^{-\frac{3}{2}}], & K_{\frac{1}{2}}[r^{\frac{3}{2}}(1+s)+1-s]. \end{array}\right\} \tag{7.1}$$

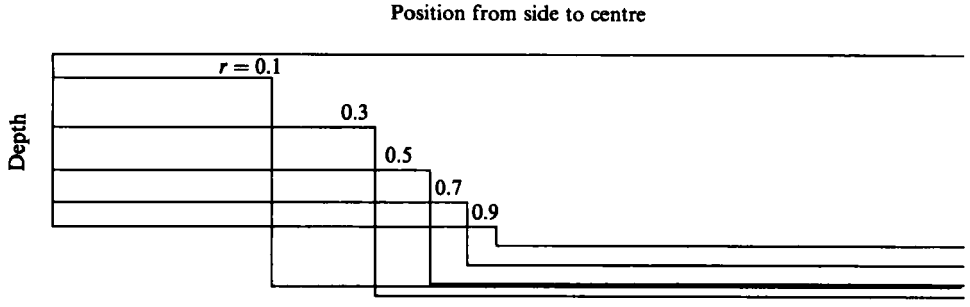

FIGURE 2. Family of depth profiles with depth ratios $1:r$ and volume flux ratios $1:r^2$ between the centre and side sections.

Here B is the distance from the centreline to the sides, $\overline{h}$ the mean depth, and $\overline{u}$ the mean or bulk velocity. The representation for the diffusivity is based upon the observation that typically κ scales as the product hu. The quantity K has the dimensions and magnitude of a transverse diffusivity.

For algebraic convenience we choose the y-coordinate to correspond with the fractional volume, integrated out from the centreline $y = 0$:

$$m_2 = \frac{2B}{1+s+(1-s)r^{-\frac{3}{4}}}, \quad \frac{2B}{(1+s)r^{\frac{3}{4}}+1-s}. \tag{7.2}$$

Hence, the depth transition is at $y = \frac{1}{2}(1+s)$, and the channel boundary is at $y = 1$. The resulting equations (3.4) for the time-lag function $G = G_+ = G_-$ become

$$r^{-2}\frac{\mathrm{d}^2G}{\mathrm{d}y^2} = (1-s)\mathscr{G} \quad \text{for } 0 < y < \tfrac{1}{2}(1+s), \tag{7.3a}$$

$$r^2\frac{\mathrm{d}^2G}{\mathrm{d}y^2} = -(1+s)\mathscr{G} \quad \text{for } \tfrac{1}{2}(1+s) < y < 1, \tag{7.3b}$$

with

$$G = G, \quad r^{-2}\frac{\mathrm{d}G}{\mathrm{d}y} = r^2\frac{\mathrm{d}G}{\mathrm{d}y} \quad \text{across } y = \tfrac{1}{2}(1+s), \tag{7.3c}$$

$$\frac{\mathrm{d}G}{\mathrm{d}y} = 0 \quad \text{on } y = 0, 1, \tag{7.3d}$$

and

$$\int_0^1 G\,\mathrm{d}y = 0, \tag{7.3e}$$

where for clarity the dimensional factors of G are carried by the quantity $\mathscr{G}$:

$$\mathscr{G} = \frac{B^2}{K}\frac{4(r^{-\frac{1}{2}}-1)}{r^2(1+s+(1-s)r^{-\frac{3}{4}})^3}. \tag{7.3f}$$

The solution for G is given by

$$\frac{G}{\mathscr{G}} = \tfrac{1}{2}(1-s)r^2[y^2-\tfrac{1}{4}(1+s)^2]+\frac{1-s^2}{24}\left((1+s)^2r^2-\frac{(1-s)^2}{r^2}\right) \quad \text{for } 0 < y < \tfrac{1}{2}(1+s), \tag{7.4a}$$

$$\frac{G}{\mathscr{G}} = -\tfrac{1}{2}(1+s)r^2((1-y)^2-\tfrac{1}{4}(1-s)^2)+\frac{1-s^2}{24}\left((1+s)^2r^2-\frac{(1-s)^2}{r^2}\right) \quad \text{for } \tfrac{1}{2}(1+s) < y < 1. \tag{7.4b}$$

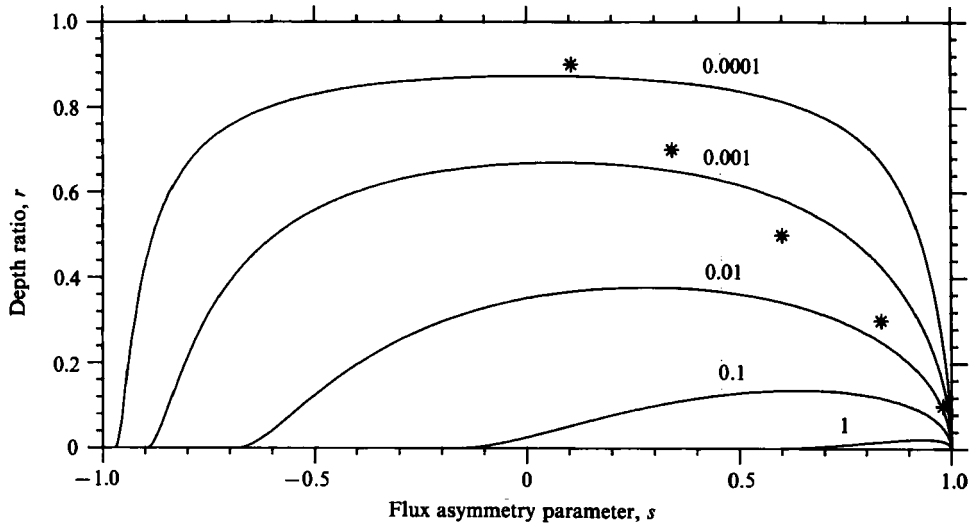

FIGURE 3. Contours of the non-dimensional longitudinal dispersion coefficient $DK/\overline{m}_1^2\overline{u}^2B^2$ as a function of topography parameters r, s. The asterisks show the (r, s)-values for the depth profiles illustrated in figure 2.

It is straightforward to evaluate the integrals required for the two-equation model

$$\frac{\overline{G}}{\mathscr{G}} = \frac{(r^{-\frac{1}{2}}-1)(1-s^2)^2}{24(1+s+(1-s)r^{-\frac{1}{2}})}\left\{(1+s)r^2+\frac{1-s}{r^2}\right\}, \tag{7.5a}$$

$$\frac{[G^2]}{\mathscr{G}^2} = (1-s^2)^2\left\{\frac{1}{240}\left(r^4(1+s)^3+\frac{(1-s)^3}{r^4}\right)-\frac{1}{576}\left((1+s)^3r^2-\frac{(1-s)^2}{r^2}\right)^2\right\}, \tag{7.5b}$$

$$\frac{\overline{G^2}-[G^2]}{\mathscr{G}^2} = \frac{(r^{-\frac{1}{2}}-1)(1-s^2)^3}{1+s+(1-s)r^{-\frac{1}{2}}}\frac{1}{1440}\left((1+s)r^2+\frac{1-s}{r^2}\right)\left(\frac{(1-s)(1+5s)}{r^2}-(1+s)(1-5s)r^2\right). \tag{7.5c}$$

We note that there are several simplifications if r and s are related:

$$s = \frac{1-r^2}{1+r^2}, \quad \text{i.e.} \ \frac{1-s}{1+s} = r^2 \tag{7.6}$$

(see figure 2). This special family of profiles is given greater emphasis in the next section.

From (3.6), (7.3f) we see that the dispersion coefficient D scales as $\overline{m}_1^2\overline{u}^2B^2/K$. Figure 3 gives contours for the precise numerical factor. Without loss of generality, the results have been restricted to $0 < r < 1$. If it should happen that the side regions are deeper than the central region, then it suffices to replace r by r^{-1} and s by $-s$. Although the dispersion coefficient does not appear explicitly in the present two-equation model, it does given an easily understood and direct measure of the efficiency of the dispersion process. In particular, there is extreme sensitivity to the precise value of the depth ratio r.

Proceeding to the two-equation model (6.1a, b), figure 4 gives a contour plot of the 'slowness factor' $\overline{G^2}/[G^2]$. A noteworthy feature exhibited in figure 4 is that when there is comparatively little flow in the deeper central region (i.e. s negative), the 'slowness factor' can be less than 1 and the temporal skewness negative (see equation

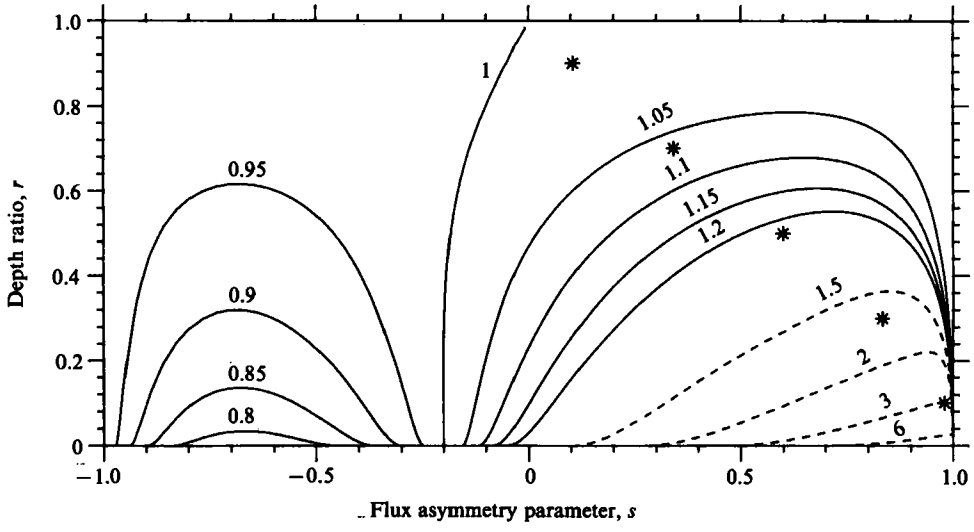

FIGURE 4. Contours of the 'slowness' of the c_1 mode (i.e. the bulk velocity $\overline{u}$ divided by the velocity u_{11} of the c_1 mode.)

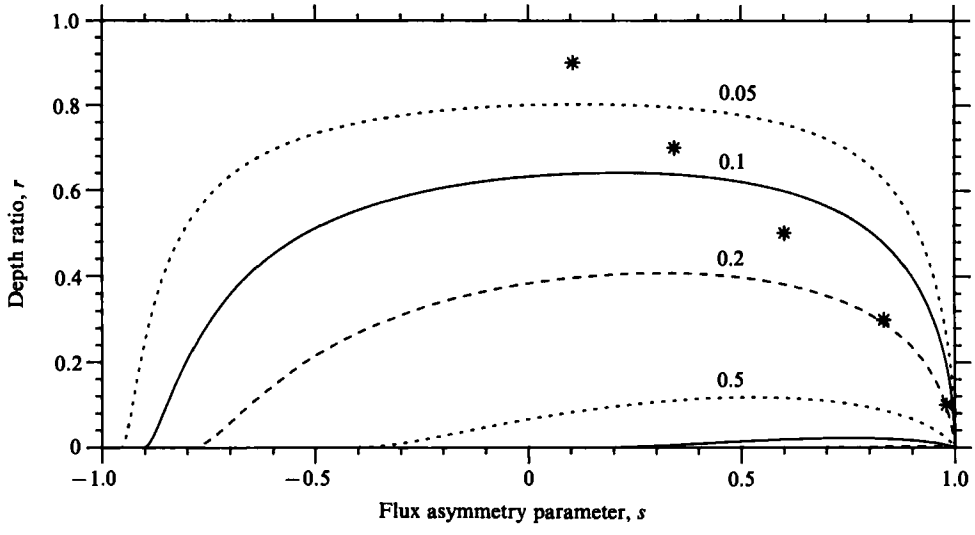

FIGURE 5. Contours of the transfer coefficient $\overline{G}/[G^2]^{\frac{1}{2}}$ for interaction between the [c] and c_1 contributions to the concentration distribution.

(3.7)). Thus, the characteristic positive temporal skewness for natural streams (Nordin & Sabol 1974) can be attributed to the typical depth profile which has the bulk of the flow in the deeper parts. The slowness, and hence the skewness, is most marked when there is a narrow shallow sill (the bottom right-hand corner of figure 4).

Figures 5 and 6 give contour plots of the transfer coefficient $\overline{G}/[G^2]^{\frac{1}{2}}$ and the non-dimensional spatial decay rate

$$\mu B^2 \overline{m}_1 \overline{u}/K. \tag{7.7a}$$

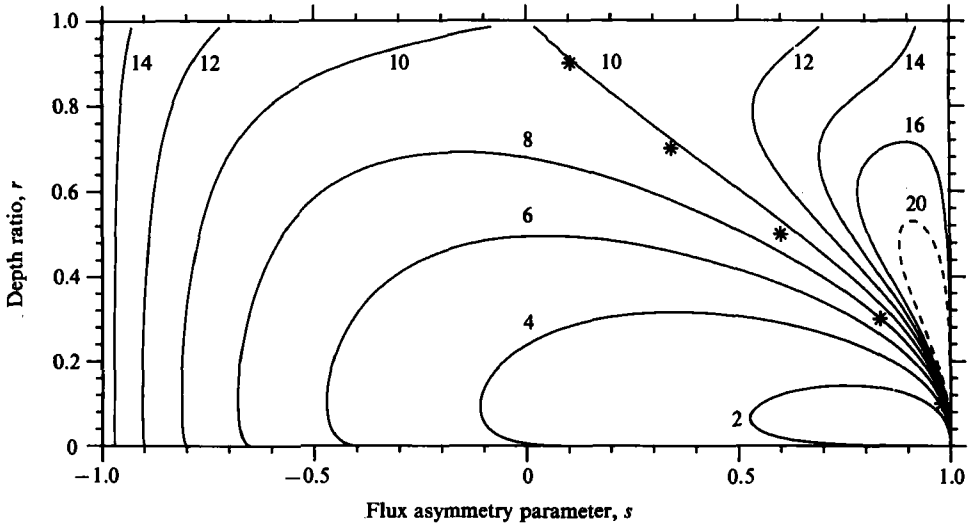

FIGURE 6. Contours of the non-dimensional spatial decay rate $\mu B^2 \overline{m}_1 \overline{u}/K$ for the c_1 mode.

As in figure 3, the dependence is principally upon the depth ratio r, but with much reduced sensitivity.

The experiments of Sumer (1976) suggest that κ scales as $0.15hu_*$, where the friction velocity u_* is about $\frac{1}{15}$ of the longitudinal velocity $m_1 u$. Hence, the dimensionless expression (7.7a) is independent of the flow rate F and is of the order

$$100\mu B^2/\overline{h}. \tag{7.7b}$$

A typical value of 10 (see figure 6) corresponds to an e-folding distance of $10B^2/\overline{h}$, which for an 10:1 breadth-to-depth ratio is $100B$ downstream. The significance of this lengthscale is that at much shorter distances (say $10B$), the cross-stream concentration profile cannot be adequately represented by just the $[c]$ and c_1 modes. While, at very much larger distances (say $1000B$), the skewness becomes small and a diffusion model is adequate. For a river with $B = 100$ m, this window of relevance for the two-equation models extends from 1 km to 100 km downstream of a discharge.

Throughout this paper, great emphasis has been placed on the importance of being able to adapt a model to different flow conditions. Thus, it warrants reiteration that, with the exception of $\overline{u}$, all the coefficients arising in the two-equation model are almost independent of the river volume flow rate F. Of course, the water depth has a weak (square-root) dependence upon F. So, the r and s values need to be adjusted. However, the only substantial changes in the model equations (6.1a, b) or (7.4) are in the explicit $\overline{u}$ velocity terms. Indeed, the precise representation of the spatial decay term μ was designed to achieve such robustness to changed flow conditions. The next section reveals similar resilience to longitudinal non-uniformity.

By contrast, in a diffusion model (3.8) the conversion factor relating the dispersion coefficient D to the non-dimensional results in figure 3, scales as F. Also, the extreme sensitivity of D to the depth ratio r would make interpolation difficult when the river varies from section to section. The relationship

$$\frac{DK}{\overline{m}_1^2 \overline{u}^2 B^2} = \frac{\overline{G}^2}{[G^2]}\left(\frac{K}{\mu B^2 \overline{m}_1 \overline{u}}\right) \tag{7.8}$$

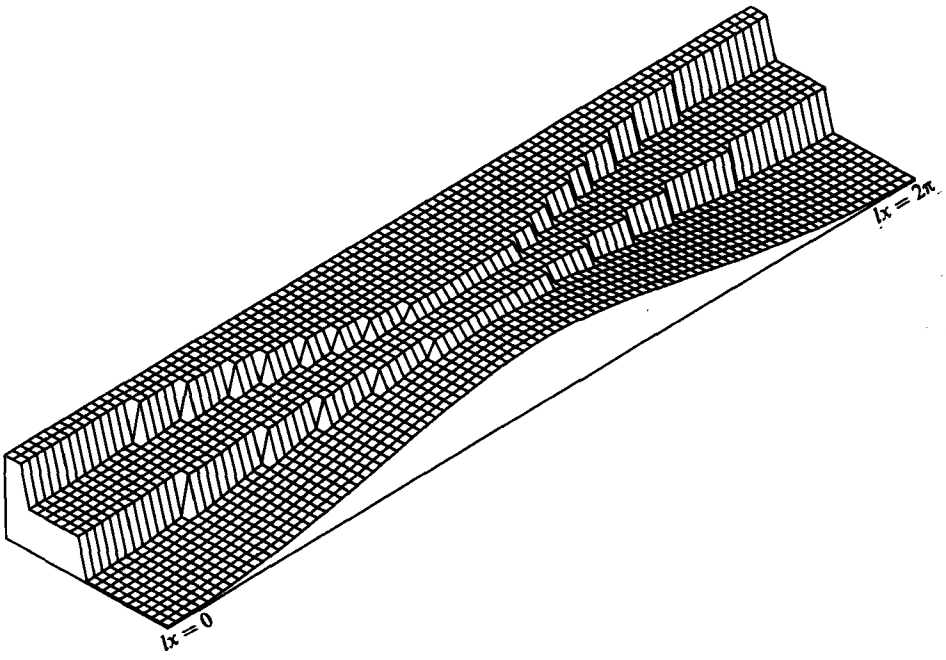

FIGURE 7. Perspective view of a self-similar depth profile as sliced along the centreline. The parameters specifying this particular geometry are $r = \frac{1}{2}, s = \frac{3}{5}, \epsilon = \frac{7}{9}$.

relates the results in figure 3 to those of figures 5 and 6. Hence the sensitivity of the dispersion coefficient D to r is shared out and greatly reduced in the two-equation model.

8. Self-similar depth profiles

We now modify the two-region geometry studied in the previous section, to permit variation of depth and breadth. However, we require that the depth ratio $1:r$ and the division of the volume flow $1+s:1-s$ between the central region and the sides remain constant (see figure 7). Mass conservation imposes the relationship

$$2\overline{m}_1 \overline{u}\overline{h}B = F = \text{constant}. \tag{8.1}$$

To cope with the x-dependence of G_+, G_- we utilize the eigenmodes. The symmetry of the geometry allows us to ignore the antisymmetric modes, and the self-similarity makes the modes independent of x:

$$\phi_n = p_n \cos(\lambda_n r y) \quad \text{for } 0 < y < \tfrac{1}{2}(1+s), \tag{8.2a}$$

$$\phi_n = (-1)^n q_n \cos(\lambda_n r^{-1}(1-y)) \quad \text{for } \tfrac{1}{2}(1+s) < y < 1, \tag{8.2b}$$

where

$$\sin\left\{\tfrac{1}{2}\lambda_n\left(r(1+s)+\frac{1-s}{r}\right)\right\} = \frac{r^2-1}{r^2+1}\sin\left\{\tfrac{1}{2}\lambda_n\left(r(1+s)-\frac{(1-s)}{r}\right)\right\}, \tag{8.2c}$$

$$p_n = \left\{\frac{1}{2}+\frac{(1-s)(r^{-4}-1)}{4}\sin^2\left(\frac{\lambda_n}{2r}(1-s)\right)\right\}^{-\frac{1}{2}}, \tag{8.2d}$$

$$q_n = \left\{\frac{1}{2} + \frac{(1+s)(r^4-1)}{4}\sin^2\left(\frac{\lambda_n r}{2}(1+s)\right)\right\}^{-\frac{1}{2}}, \tag{8.2e}$$

$$\overline{\phi}_n = \frac{-2(r^{-\frac{1}{2}}-1)\,p_n \sin\left(\frac{1}{2}\lambda_n r(1+s)\right)}{\lambda_n r(1+s+(1-s)r^{-\frac{1}{2}})}, \tag{8.2f}$$

$$\overline{\phi_n \phi_m} = \frac{-(r^{-\frac{1}{2}}-1)\,p_m p_n}{r(1+s+(1-s)r^{-\frac{1}{2}})}\left\{\frac{\sin\left[\frac{1}{2}(\lambda_n-\lambda_m)r(1+s)\right]}{\lambda_n-\lambda_m} + \frac{\sin\left[\frac{1}{2}(\lambda_n+\lambda_m)r(1+s)\right]}{\lambda_n+\lambda_m}\right\} \quad (m \neq n), \tag{8.2g}$$

$$\overline{\phi_n^2} = \frac{1}{1+s+r^{-\frac{1}{2}}(1-s)}\{2r^{-\frac{1}{2}} - \tfrac{1}{2}(r^{-\frac{1}{2}}-1)\,p_n^2(1+s+\sin[\lambda_n r(1+s)])\}. \tag{8.2h}$$

The roots λ_n can be arranged in sequence:

$$(n-\tfrac{1}{2})\pi < \frac{\lambda_n}{2}\left(r(1+s)+\frac{1-s}{r}\right) < (n+\tfrac{1}{2})\pi. \tag{8.3}$$

The x-dependence arises in the decay rate

$$\mu_n = \lambda_n^2 \frac{K}{B^2 \overline{u}\,\overline{m}_1}\frac{r^2[1+s+(1-s)r^{-\frac{3}{2}}]^3}{4[1+s+(1-s)r^{-\frac{1}{2}}]}. \tag{8.4}$$

To solve for the amplitudes $t_n^{(+)}, t_n^{(-)}$ in the eigenfunction expansions (5.1a, b), we need to evaluate the double integrals (5.1c, d).

These can be simplified if the decay exponents $\overline{m}_1\mu_n$ are made independent of x. From (8.4) and mass conservation (8.1) we see that this implies a particular distortion for the longitudinal coordinate:

$$\overline{m}_1 = \frac{B}{\overline{h}K}\frac{h_0\kappa_0}{B_0}. \tag{8.5}$$

The remaining $1/\overline{u}$ integrands in (5.1c, d) are also influenced by this coordinate distortion. Mass conservation, together with the scaling of K as $0.01\overline{m}_1\,\overline{u}\overline{h}$ enables us to relate $1/\overline{u}$ to $B(x)^3$. Thus, as was noted by Smith (1983, §9), it is breadth changes that are important as regards the memory character of the dispersion process. Moreover, the cubic dependence of $t_n^{(+)}, t_n^{(-)}$ upon $B(x)$ gives an exaggerated response to breadth changes.

As a specific example we take

$$\left.\begin{aligned} B = B_0(1+\epsilon\cos lx)^{\frac{1}{3}}, \quad \overline{h} = h_0(1+\epsilon\cos lx)^{\frac{2}{3}}, \\ K = \kappa_0(1+\epsilon\cos lx)^{-\frac{1}{3}}, \quad \overline{m}_1 = 1, \quad \overline{u} = u_0(1+\epsilon\cos lx)^{-1}. \end{aligned}\right\} \tag{8.6}$$

Here ϵ is a measure of the topographic changes, and l is the longitudinal wavenumber. The formulae (5.1c, d) become

$$t_n^{(+)} = \frac{\overline{\phi}_n}{u_0\mu_n}\left\{1+\epsilon\frac{(\mu_n^2\cos lx + \mu_n l\sin lx)}{\mu_n^2+l^2}\right\}, \tag{8.7a}$$

$$t_n^{(-)} = \frac{\overline{\phi}_n}{u_0\mu_n}\left\{1+\epsilon\frac{(\mu_n^2\cos lx - \mu_n l\sin lx)}{\mu_n^2+l^2}\right\}. \tag{8.7b}$$

The memory effects give a phase lag in $t_n^{(+)}$ and a phase lead in $t_n^{(-)}$ relative to the breadth changes. To simplify the presentation of numerical results, figure 7 and the subsequent figures are restricted to the case

$$\epsilon = \tfrac{7}{9}. \tag{8.8}$$

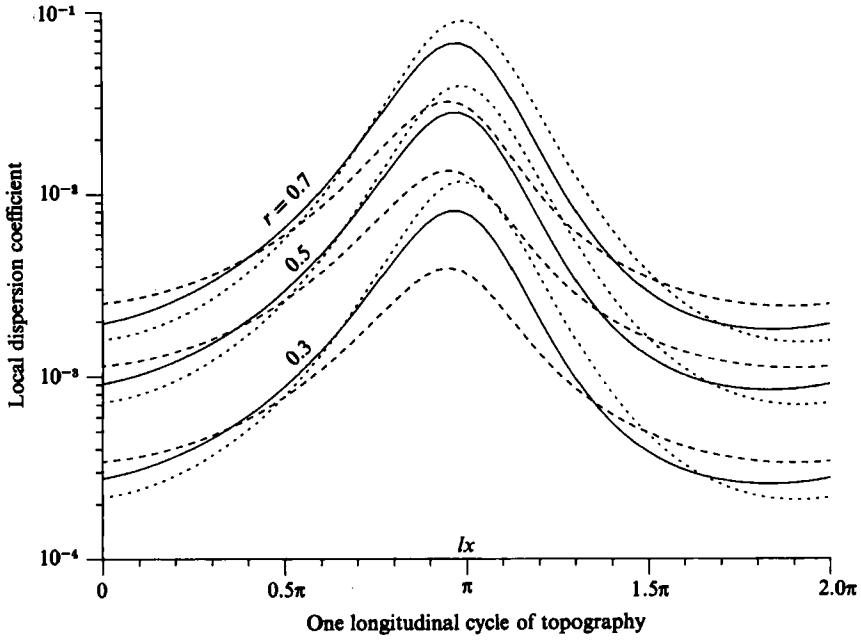

FIGURE 8. Logarithmic graph of the local longitudinal shear dispersion coefficient for the three depth ratios $r = 0.7, 0.5, 0.3$ and for topographic changes which by comparison with the rate of lateral mixing are short (· · · · · ·), moderate (——), or long (– – –).

Thus, along the flow the breadth changes by a factor of two, with a factor-of-four depth change, i.e. large enough to be realistic.

From (8.2) we note that, if r and s are related,

$$s = \frac{1-r^2}{1+r^2} \tag{8.9}$$

(see figure 2), then there are major simplifications. In particular, $\overline{\phi}_{2n} = 0$, so we need only consider the ϕ_{2n+1} modes:

$$\left.\begin{aligned} \lambda_{2n+1} &= (n+\tfrac{1}{2})\,\pi(r^{-1}+r), \quad p_{2n+1} = 2^{\frac{1}{2}}r, \\ q_{2n+1} &= 2^{\frac{1}{2}}r^{-1}, \quad \overline{\phi}_{2m+1} = \frac{(-1)^{n+1}2^{\frac{1}{2}}(r^{\frac{1}{2}}-r)}{(n+\frac{1}{2})\,\pi(1+r^{\frac{3}{2}})}, \\ \overline{\phi_{2n+1}\phi_{2m+1}} &= 0 \quad (n \neq m), \quad \overline{\phi^2_{2n+1}} = \frac{r^2+r^{-\frac{1}{2}}}{1+r^{\frac{3}{2}}}. \end{aligned}\right\} \tag{8.10}$$

All subsequent results are restricted to this family of depth topographies. We remark that the 3:1 ratio between the λ-values for $n = 1, n = 0$ implies a 1:9 ratio between the corresponding e-folding distances.

As a precursor to the two-equation modelling, figure 8 shows the non-dimensional shear dispersion coefficient

$$D\kappa_0/u_0^2 B_0^2. \tag{8.11}$$

The nine curves correspond to the three-depth ratios $r = 0.7, 0.5, 0.3$ and to the three non-dimensional topographic wavenumbers $L = 3, 10, 30$, where

$$L = \frac{lB_0^2 u_0}{\kappa_0} \approx 100l\frac{B_0^2}{h_0}, \tag{8.12}$$

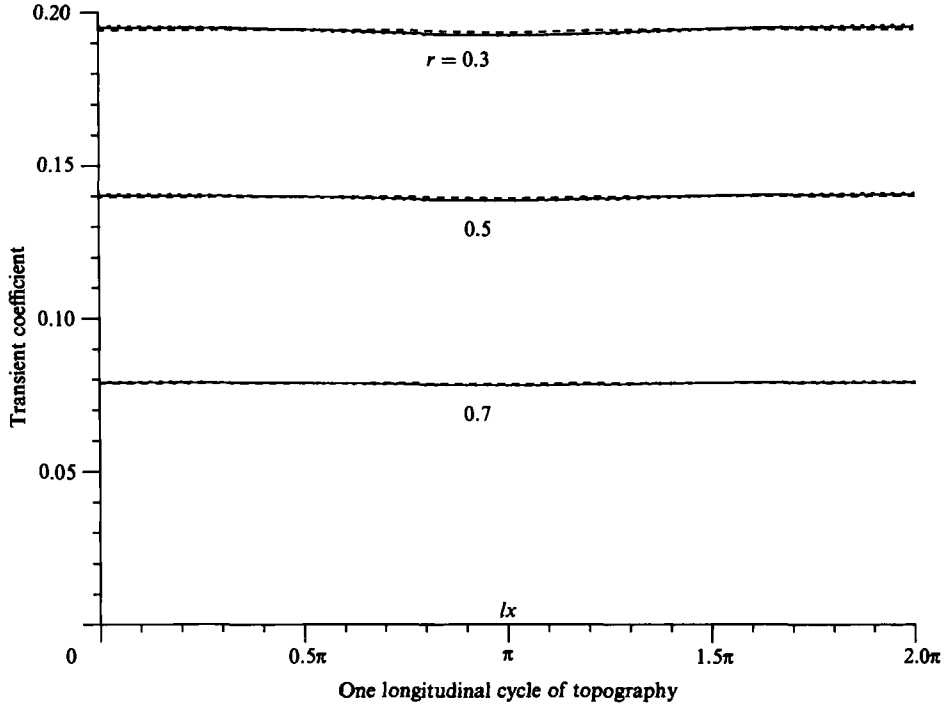

FIGURE 9. The x-dependence of the transfer coefficient when the depth ratio has the values $r = 0.7, 0.5, 0.3$ and for non-dimensional topographic wavenumbers $L = 30$ (· · · · · ·), 10 (——), 3 (– – –).

i.e. long, moderate and short lengthscales relative to the diffusion length associated with the c_1 mode. In all cases, the values of D exhibit marked variations with respect to x (by up to a factor of 64). As in figure 4, there is also extreme sensitivity to the depth ratio r. It is these wide ranges of values of D which necessitated a logarithmic plot.

It is now straightforward to perform the summations (5.2*a–e*) and to evaluate the cross-sectional integrals $[G_+ G_-], \overline{G}_+, \overline{G_+ G_-}$, etc. In particular, we find that the slowness factor is independent of x:

$$\frac{\overline{G_+ G_-}}{[G_+ G_-]} = \frac{r^2 + r^{-\frac{1}{2}}}{1 + r^{\frac{3}{2}}}. \tag{8.13}$$

In the three depth ratios $r = 0.7, 0.5, 0.3$ the respective slowness values are 1.06, 1.23, 1.65.

Figures 9 and 10 show the x-dependence of the transfer coefficient $(\overline{G}_+ \overline{G}_- / [G_+ G_-])^{\frac{1}{2}}$ and of the non-dimensional spatial decay rate

$$\mu B_0^2 u_0 \kappa_0 \approx 100 \mu \frac{B_0^2}{h_0}. \tag{8.14}$$

More usually μ varies as h/B^2. It happens that, for the particular geometry (8.6), the quantity h/B^2 is constant, and μ is virtually independent of x.

The general implications that can be inferred from the above illustrative

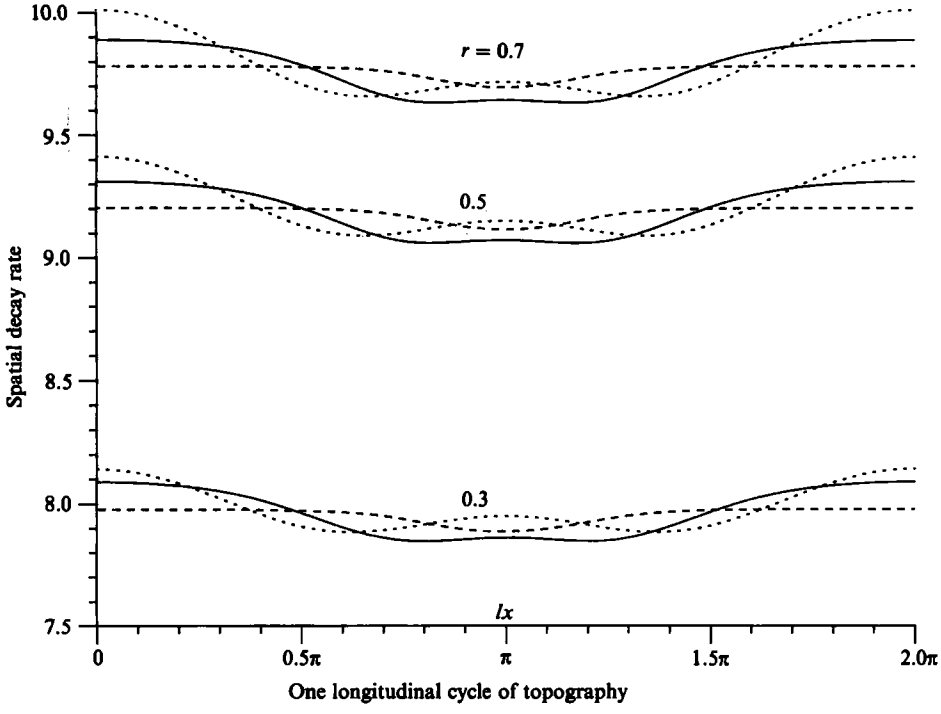

FIGURE 10. The x-dependence of the non-dimensional spatial decay rate when the depth ratio has the values $r = 0.7, 0.5, 0.3$ and for short- (·····), moderate- (——), or long- (– – –) wavelength topographic changes.

example, are that in the model equations (6.1a, b), the coefficients $[G_+ G_-]/\overline{G_+ G_-}$, $(\overline{G_+}\,\overline{G_-}/[G_+ G_-])^{\frac{1}{2}}$, μ do not vary very much. The principal x-dependence and flow-dependence is in the explicit $\overline{u}$ terms.

9. Concluding remarks

This work is based upon the premise that pollution prediction methods based upon field observations or upon hydrodynamics should be identical. The starting point was the empirical dead-zone model (1.1a, b) used by Beer & Young (1983). The present analysis, based upon the hydrodynamics, leads to the suggestion of a closely related model (6.1a, b). Depending upon circumstances, the coefficients in that model could be evaluated either from field observations or from equations for advection and diffusion. It is when flow conditions change (floods, droughts, land reclamation or dredging) that the hydrodynamic basis is important, in ensuring the continued applicability of the pollution-prediction model.

Dr Fu Jia of the Chinese Academy of Sciences, Beijing, with his concern about the Yangtze, asked the key questions which stimulated this work. Financial support was given by the Royal Society.

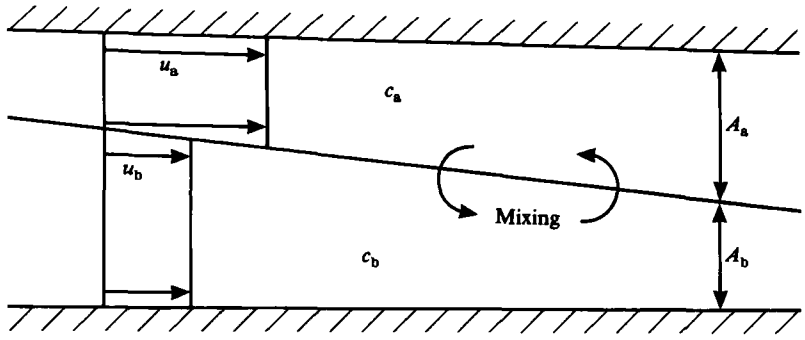

FIGURE 11. Sketch of a two-layer flow with a varying division of the total volume flux between the two well-mixed layers.

Appendix. Two well-mixed zones

Figure 11 shows two well-mixed zones with areas A_a, A_b and velocities u_a, u_b. The equations for the concentrations c_a, c_b in these two zones are

$$\partial_t(A_a c_a)+A_a u_a \partial_x c_a = A_a Q_a+(\overline{m}_1 \overline{u} A\Lambda+H(\partial_x(A_a \overline{m}_1 u_a))\frac{1}{\overline{m}_1}\partial_x(A_a \overline{m}_1 u_a))(c_b-c_a), \tag{A 1a}$$

$$\partial_t(A_b c_b)+A_b u_b \partial_x c_b = A_b Q_b+(\overline{m}_1 \overline{u} A\Lambda+H(\partial_x(A_b \overline{m}_1 u_b))\frac{1}{\overline{m}_1}\partial_x(A_b \overline{m}_1 u_b)(c_a-c_b). \tag{A 1b}$$

Here Q_a, Q_b are the source strengths, Λ an exchange coefficient, and the Heaviside function terms allow for the varying division of volume flux between the two zones. The dead-zone model (1.1a, b) is a special case with

$$u_a = u, \quad u_b = 0, \quad A_a = \frac{\beta}{\alpha+\beta}A, \quad A_b = \frac{\alpha}{\alpha+\beta}A, \quad \Lambda = \frac{\alpha}{u}. \tag{A 2}$$

To convert the two-equation model (5.4a, b) to the form (A 1a, b), we need to diagonalize the ∂_t and ∂_x terms. To do this, we define the combination variables

$$c_a = [c]-\frac{\xi}{1+\gamma}c_1, \quad c_b = [c]+\frac{\xi}{1-\gamma}c_1. \tag{A 3a, b}$$

The necessary choices for the parameters ξ, γ can be shown to be

$$\xi = (\gamma-\delta)/\overline{\Phi}_-, \tag{A 4a}$$

with
$$\gamma = \frac{\overline{G_+ G_-}-[G_+ G_-]}{\{(\overline{G_+ G_-}-[G_+ G_-])^2+4\overline{G}_+ \overline{G}_-[G_+ G_-]\}^{\frac{1}{2}}}, \tag{A 4b}$$

and
$$\delta = \frac{\overline{G_+ G_-}-[G_+ G_-]-2\overline{G}_+ \overline{G}_-}{\{(\overline{G_+ G_-}-[G_+ G_-])^2+4\overline{G}_+ \overline{G}_-[G_+ G_-]\}^{\frac{1}{2}}}. \tag{A 4c}$$

In terms of ξ, γ, δ the two-zone flow can be specified

$$A_a = \tfrac{1}{2}(1+\delta)A, \quad A_b = \tfrac{1}{2}(1-\delta)A, \tag{A 5a, b}$$

$$A_a u_a = \tfrac{1}{2}(1+\gamma)A\overline{u}, \quad A_b u_b = \tfrac{1}{2}(1-\gamma)A\overline{u}, \tag{A 5c, d}$$

$$A_a Q_a = \tfrac{1}{2}(1+\gamma)\overline{q}A-\tfrac{1}{2}(\gamma-\delta)\frac{\overline{qG_-}}{\overline{G}_-}A, \tag{A 5e}$$

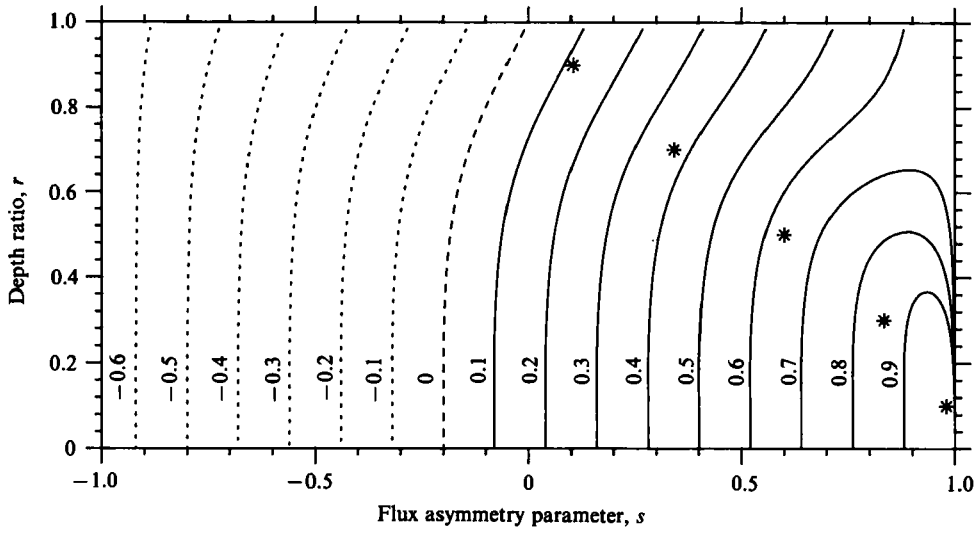

FIGURE 12. Contours of the flux asymmetry coefficient γ in the two-zone model as a function of the depth ratio r and the actual flux asymmetry s.

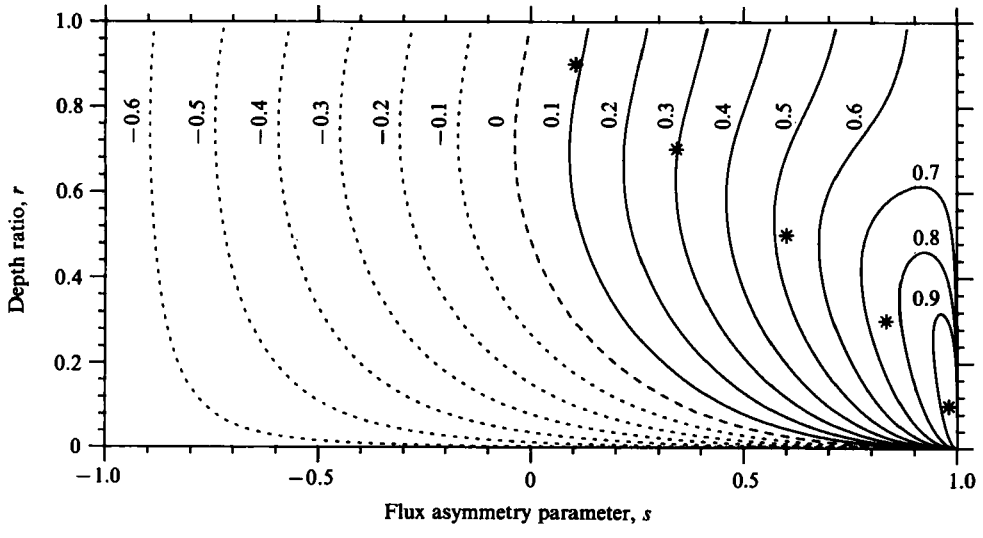

FIGURE 13. Contours of the area asymmetry coefficient δ in the two-zone model.

$$A_b Q_n = \tfrac{1}{2}(1-\gamma)\bar{q}A + \tfrac{1}{2}(\gamma-\delta)\frac{\overline{qG_-}}{\bar{G}_-}A, \tag{A 5f}$$

$$\Lambda = \tfrac{1}{4}(1-\gamma^2)\left(\mu - \frac{2}{\bar{m}_1}\frac{\partial_x \xi}{\xi}\right) - \frac{1}{4\bar{m}_1}(\operatorname{sgn}(\partial_x \gamma)+\gamma)\,\partial_x \gamma. \tag{A 5g}$$

The dead-zone model (1.1a, b) corresponds to

$$\gamma = 1, \quad \delta = \frac{\beta-\alpha}{\alpha+\beta}. \tag{A 6a, b}$$

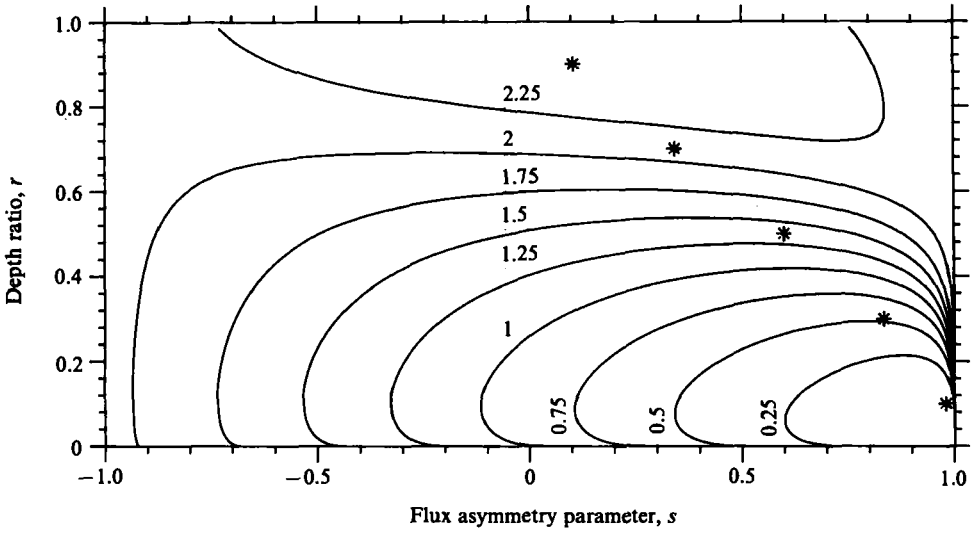

FIGURE 14. Contours of the non-dimensional exchange coefficient $AB^2\overline{m}_1\,\overline{u}/K$ for the equilibration of the zone concentrations in the two-zone model.

The two-zone character of the flow investigated in §7 makes the comparison with the two-zone model particularly intriguing. If the actual flow was well-mixed in each zone, then we could identify s with γ. Figure 12 shows that the more gentle mixing in the actual flow makes γ weakly dependent upon the depth ratio r. For s greater than 0.5 the large value of γ indicates that in this regime the dead-zone model yields results close to those of the new two-equation model. The direct counterpart of the area asymmetry parameter δ is

$$\frac{1+s-(1-s)\,r^{-\frac{1}{2}}}{1+s+(1-s)\,r^{-\frac{1}{2}}}. \tag{A 7}$$

Figure 13 reveals that the δ-contours are qualitatively similar to this formula (e.g. the position and shape of the $\delta = 0$ contour). However, the (r, s)-dependence is generally weaker (e.g. along $r = 1$ neither γ nor δ have the full range from -1 to 1). Figure 14 shows contours of the non-dimensional exchange coefficient

$$\frac{AB^2\overline{m}_1\,\overline{u}}{K} \approx 100\frac{AB^2}{\bar{h}}. \tag{A 8}$$

We note that this scaling for A is independent of the river volume flow rate F. Hence, for varied flow rate the only changes to the two-zone equations (A 1a, b) are in the explicit velocity terms $u_a, u_b, \overline{u}$.

For uniform flows there is a choice between the use of temporal and of spatial moments. This leads to a choice between the two-mode model (6.1a, b) derived above and that derived by Smith (1981, §5). The coefficients in the respective models are not the same. However, neither are the choices $[c]$ and $\bar{c}$ for the principal dependent variable. This particular source of difference disappears in the respective two-zone formulations. For uniform flows the functions G_+, G_- are equal and can be related to the centroid displacement function $g(y, z)$ which arises in the use of spatial moments (Smith 1984, §11). In this way it can be confirmed that the two-zone specification

(A 4), (A 5) is the same as that given by Smith (1981, equations (5.11)–(5.13)). Hence, in the limit of longitudinally uniform flows, the two-zone version (A 1*a*, *b*) of the present model is identical with its predecessor.

REFERENCES

BEER, T. & YOUNG, P. C. 1983 Longitudinal dispersion in natural streams. *J. Env. Engng* **109**, 1049–1067.

CHATWIN, P. C. 1970 The approach to normality of the concentration distribution of a solute in solvent flowing along a straight pipe. *J. Fluid Mech.* **43**, 321–352.

CHATWIN, P. C. 1980 Presentation of longitudinal dispersion data. *J. Hydraul. Div. ASCE* **106**, 71–83.

FISCHER, H. B. 1969 The effects of bends on dispersion in streams. *Wat. Resources Res.* **5**, 496–506.

NORDIN, C. F. & SABOL, G. V. 1974 Empirical data on longitudinal dispersion in rivers. *U.S. Geological Survey. Rep. no.* 20-74. 372 pp.

SMITH, R. 1981 A delay-diffusion description for contaminant dispersion. *J. Fluid Mech.* **105**, 469–486.

SMITH, R. 1983 Longitudinal dispersion coefficients for varying channels. *J. Fluid Mech.* **130**, 299–314.

SMITH, R. 1984 Temporal moments at large distances downstream of contaminant releases in rivers. *J. Fluid Mech.* **140**, 153–174.

SUMER, S. M. 1976 Transverse dispersion in partially stratified tidal flow. *Univ. California Berkley, Hydraul. Engng, Lab. Rep.* WHM-20.

TAYLOR, G. I. 1953 Dispersion of soluble matter in solvent flowing slowly through a tube. *Proc. R. Soc. Lond.* A **219**, 186–203.

YOTSUKURA, N. & SAYRE, W. W. 1976 Transverse mixing in natural channels. *Wat. Resources Res.* **12**, 695–704.